Alexandria Engineering Journal (2022) 61, 9891–9900

HOSTED BY

Alexandria University

Alexandria Engineering Journal

www.elsevier.com/locate/aej
www.sciencedirect.com

Novel approach of anti-resonant fiber with supporting 64 orbital angular momentum modes for optical communication

Md. Mehedi Hassan [a,f], Lway Faisal Abdulrazak [b], Abdullah G. Alharbi [c], Kawsar Ahmed [a,d,*], Francis M. Bui [d], Fahad Ahmed Al-Zahrani [e], Muhammad Shahin Uddin [a]

[a] *Group of Bio-photomatiχ, Department of Information and Communication Technology, Mawlana Bhashani Science and Technology University, Santosh, Tangail 1902, Bangladesh*
[b] *Department of Computer Science, Cihan University Sulaimaniya, Sulaimaniya 46001, Kurdistan Region, Iraq*
[c] *Department of Electrical Engineering, Faculty of Engineering, Jouf University, Sakaka 42421, Saudi Arabia*
[d] *Department of Electrical and Computer Engineering, University of Saskatchewan, 57 Campus Drive, Saskatoon, SK S7N 5A9, Canada*
[e] *Computer Engineering Department, Umm Al-Qura University, Mecca 24381, Saudi Arabia*
[f] *Department of Computing and Information System (CIS), Daffodil International University, Dhaka 1341, Bangladesh*

Received 15 December 2021; revised 19 January 2022; accepted 4 March 2022
Available online 29 March 2022

KEYWORDS

Anti-resonant fiber;
Fiber optics communication;
Negative curvature fiber;
Orbital angular momentum;
Mode quality;
Flat dispersion

Abstract A novel single material-based anti-resonant fiber is designed, investigated, and explored in this article with supports of up to 64 OAM modes over the 0.6 μm to 1.0 μm as operating wavelength. The other properties of the designed fiber including confinement loss (CL), OAM purity, effective refractive index differences (ERIDs), and dispersion variations provide the exceptional output. This fiber, the CL approximately varies between the 5.7031×10^{-5} dB/m to 9.2537×10^{-4} dB/m, the OAM purity is 97% to 99%, the ERIDs are higher than 10^{-4} for all the modes, and the least dispersion variations is −8.838 ps/km-nm for the $EH_{1,1}$ mode. All the outstanding properties of the presented fiber are calculated using the FEM and the PML within the COMSOL Multiphysics simulator. Therefore, to the ideal of our knowledge, the proposed anti-resonant fiber is mostly applicable in the high-quality long-distance fiber communications system.

* Corresponding author at: Department of Information and Communication Technology, Mawlana Bhashani Science and Technology University, Santosh, Tangail 1902, Bangladesh.
E-mail addresses: mehedihassan.mbstu@gmail.com (Md. Mehedi Hassan), lway.faisal@sulicihan.edu.krd (L.F. Abdulrazak), a.g.alharbi@ieee.org (A.G. Alharbi), kawsar.ict@mbstu.ac.bd (K. Ahmed), francis.bui@usask.ca (F.M. Bui), fayzahrani@uqu.edu.sa (F.A. Al-Zahrani), shahin.uddin@mbstu.ac.bd (M.S. Uddin).

Peer review under responsibility of Faculty of Engineering, Alexandria University.

https://doi.org/10.1016/j.aej.2022.03.006
1110-0168

1. Introduction

Space division multiplexing (SDM) and mode division multiplexing (MDM) are being considered as potential technologies for increasing the transmission capacity of optical fiber communication systems in the face of an ever-increasing demand for bandwidth resources in the current day. To transmit independent data streams, different fiber modes like linear polarization (LP) or orbital angular momentum (OAM) modes are being investigated. Except for the inter-mode dispersion, the OAM modes created by the linear combination of odd and even modes of the identical vector eigen-mode can be considered of as a superior way for achieving multiple-input-multiple-output (MIMO) free MDM transmission [1–4]. OAM has permitted a collection of application fields such as imaging, sensing, and micro-manipulation [5–8]. The characteristics feature of OAM beams whose complex amplitude constructs the helical phase front which is indicated by '$\exp(i\ l\ \varphi)$', where, 'φ' and 'l' refer to the azimuthal angle and the topological charge that is infinite value in theory termed, respectively. Therefore, in principle, the amount of OAM-carrying beams is unbounded. It is possible to improve the spectral efficiency and data reception of optical fiber communication systems by multiplexing and demultiplexing (Mux and Demux) OAM modes, as coaxial light beams from distinct OAM states may be precisely partitioned [9,10]. Presently, ring-formation high refractive index profile fiber is broadly applied for OAM based fiber devices and communications systems because of its unique OAM mode shape. The annular shape of ring fibers prepares it adequately for conveying OAM modes as well as OAM beams' intensity profile. Sustaining the fundamental mode postulate could potentially minimize the mode crosstalk using the proper parameter choice and facilitate the processes of multiplexing and multiplexing [11–14]. Moreover, different type of stability with its applications is analyzed in neural networks [15–17]. Furthermore, the OAM modes number is a necessary property of the photonic crystal fiber (PCF) that is more impact on the fiber communication systems. For this reason, we have built a new concept fiber that supports better optical propagation features (especially confirmations of a large amount of OAM modes).

Previously, different types of PCF have been proposed such as single guided channel, double guided channel, and ring-based materials doped channel, etc. that transmission the OAM modes. An annular index profile and air core-based fiber were presented by Brunet et al., [18] with supporting the 9 orders of OAM mode and also fabricated through the MCVD method. Fujisawa et al. [19] explored the enlargement of OAM modes of light in coiled tube birefringent PCFs, where the efficient creation of OAM modes can be obtained by inverting the PCF periodically. Besides, Geng et al., [20] raised a ring-core Schott glass-based high dispersion-coupled fiber. For various OAM modes, the presented fiber indicates a large negative dispersion in the region of 1.5 μm. A new type of fiber was presented by T. He et al. that supports the 54 OAM modes over the 650 nm broad bandwidth. A high refractive index profile is inserted within the air-hole claddings (two) in the silica layer (where the OAM modes transmission) [21]. Israk et al. [22] was introduced a new coil shape structure with the two type's materials (silica and SF2 are used as a background and ring materials) as well as proposed fiber can support 56 OAM modes. A ring-based double guided low crosstalk fiber was reported by Wang et al., [23] that produces 56 OAM and 4 LP modes, however doping the high index profile (SF6 material). Two varieties of low-loss and weak-guiding OAM annular core fibers were experimentally observed by Wang et al., [24] which supports 14 and 22 Eigen mode over the 1.55 μm, respectively. It has been proven that positive curvature fibers limit light more weakly than negative curvature fibers (NCF) [24,25]. In the year of 2019, Tu et al., [1] indicated the generation of 28 OAM modes in the NCF among the infrared band, and the CL reached up to 10^{-10} – 10^{-15} dB/cm from 1.2 to 1.7 μm wavelength.

In this article, we simulate, analyze and investigate the novel approach of anti-resonant fiber with supporting 64 OAM modes and other propagation effects (such as ultralow confinement loss, and better mode quality, etc.) on the fiber communications. In the ring-core, the light constricted can be increased through the Fresnel reflection from both sides (inside and outside from the ring) negative bent glass wall, which can be defined as the anti-resonant effect, and every OAM modes are enclosed by the manner of total internal reflection (TIR). The proposed fiber will be amplified in the 400 nm bandwidth (0.6 μm to 1.0 μm) and whole the exploration has been obtained by the COMSOL Multiphysics software.

2. Structure and methodology

The two-dimensional simplified cross-sectional sketch of the raised anti-resonant fiber with supporting 64 OAM modes is displayed in Fig. 1. The three-layer structure is sheltered inside the fiber. In the first layer (outmost layer) and third layer (innermost layer), 6 circular tubes with inclination angles of 60° are connected with the fiber. In the second layer (middlemost layer), an annular region is connected with the outer and inner layer, respectively in which the OAM modes are produced. The thickness of both layers (inner and outer) tube is 0.20 μm and the annular region (r_2- r_1) is 1.00 μm. Moreover, a perfectly matching layer (PML) with 0.50 μm (r_5- r_4) thickness is used to exploit an extra electromagnetic distraction light beam on the boundary. Finally, the basic parameters of the proposed anti-resonant fiber are shown in Table 1.

The intensity distribution in different OAM modes of the anti-resonant fiber is displayed in Fig. 2. The HE mode is a less

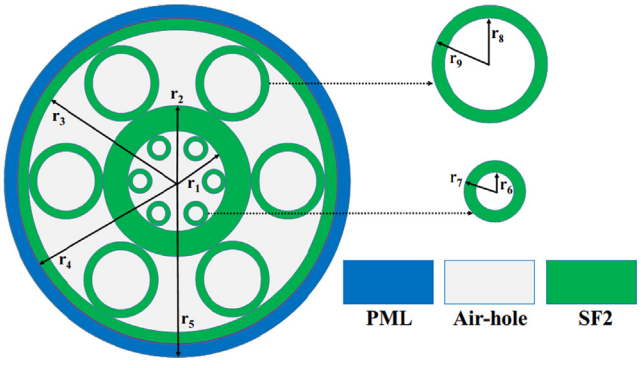

Fig. 1 Sectional view of the intended ring-based anti-resonant fiber. The meanings of r_1 – r_9 are discussed in Table 1 with their corresponding values for this study.

Table 1 Fundamental parameter of the designed anti-resonant fiber as shown in Fig. 1.

Parameter	Value (μm)
Inner ring radius, r_1	2.00
Outer ring radius, r_2	3.00
Radial radius inside the fiber, r_3	6.00
Radius of the inner PML, r_4	6.50
Radius of the outer PML, r_5	7.00
Thickness of the inner tube, r_7- r_6	0.20
Thickness of the outer tube, r_9- r_8	0.20

effective refractive index (ERI) compared to the EH mode at the irreversible wavelength of the analogous order vector modes. For this reason, we define the EH and HE modes to obtain whole the propagation characteristics of the reported fiber using the PML and the finite element method (FEM) through the simulator. Also, the vector notations of the $TE_{0,1}$ and $TM_{0,1}$ modes in Fig. 2 (corresponds to Fig. 1 as well) are indicated by the arrows (red color). Therefore, the large number of vector modes (64 OAM) is supported by the anti-resonant fiber which increases the channel capacity for the optical fiber communications.

3. Performance and result analysis of the anti-resonant fiber

HE, EH, TE, and TM are four vector modes that can be supported by a fiber with a circular symmetrical topology. Those of the modes, even and odd modes are present in both HE and EH mode and also present the phase separation among the even and odd mode is $\pm\ \pi/2$. When the ERI separation between the vector modes is less, leading to the creation of linear polarization (LP) modes and there will be evident crosstalk among the vector modes. But when the ERIDs among the vector mode are $>10^{-4}$, the OAM modes can be propagated into the fiber [18]. In this section, the following part like the supported OAM modes, mode quality, ERI, ERID, dispersion, effective area, numerical aperture, and confinement loss will be discussed with proper explanation.

3.1. Supported OAM modes

The designed anti-resonant fiber is composed of a single type of SF2 material that supports many OAM modes (operating wavelength range in between 0.6 μm and 1.0 μm). The supported OAM modes through the proposed fiber can be produced using the linear consolidation of even and odd modes of the HE and EH vector modes. However, the coordination process of adopted the OAM modes can be expressed as Eqs. (1) and (2) [26]:

$$\left\{\begin{array}{l} OAM^{\pm}_{\pm l,m} = HE^{even}_{l+1,m} \pm jHE^{odd}_{l+1,m} \\ OAM^{\mp}_{\pm l,m} = EH^{even}_{l-1,m} \pm jEH^{odd}_{l-1,m} \end{array}\right\};\ (l > 1) \tag{1}$$

$$\left\{\begin{array}{l} OAM^{\pm}_{\pm 1,m} = HE^{even}_{2,m} \pm jHE^{odd}_{2,m} \\ OAM^{\mp}_{\pm 1,m} = TM_{0,m} \pm jTE_{0,m} \end{array}\right\};\ (l = 1) \tag{2}$$

where 'l' and 'm' denote the infinity number of topological charge and radial sequence of vector modes, consecutively. The superscript and subscript '$\pm$' represent the direction of circular polarization and wave-front rotation, respectively. Higher radial order vector modes (where m is greater than 1) must be established in order to effectively create OAM modes, as the phase allocation of higher-order modes varies between regions of different annular cores. This affair creates it difficult to Mux and Demux the OAM modes and for this reason, we select the radial order mode m is equal to 1. The supported OAM modes number versus wavelength of the presented fiber is explicit in Fig. 3. In this scenario, it is clearly understood that the mode number of OAM is gradually decreasing with an increase in the wavelength. Therefore, the total number of

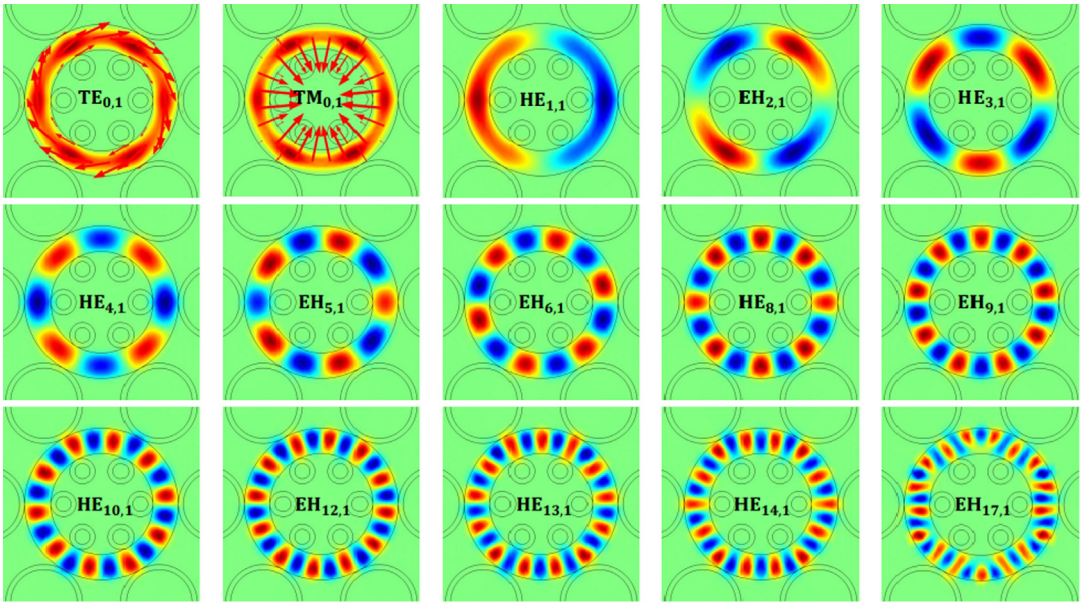

Fig. 2 Mode field intensity distribution in different vector modes of the proposed fiber.

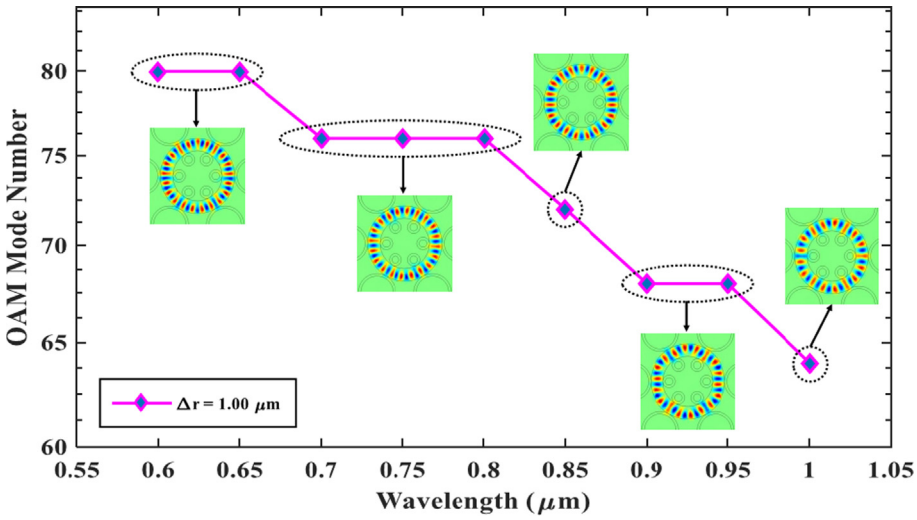

Fig. 3 OAM mode number with wavelength of the anti-resonant fiber. Five structures represent the intensity of the indicated OAM mode number.

supported OAM modes reaches up to 64 in the 400 nm bandwidth of the designed anti-resonant fiber. We hope it provides robust data transmission among the fiber communications.

3.2. OAM purity

OAM purity or mode quality is a significant propagation property that influencing OAM fiber transmission. The high purity-based OAM modes provide the efficient transmission of information and also used to apply MDM technology. The expression can be used to express the modal quality of OAM, Eq. (3) [27]:

$$\eta = \frac{I_r}{I_c} = \frac{\iint_{rings} \left|\vec{E}\right|^2 dxdy}{\iint_{cross-section} \left|\vec{E}\right|^2 dxdy} \tag{3}$$

where 'I_r' and 'I_c' define the average electric mode strength of the annular region inside the anti-resonant fiber and the 2D cross-sectional region of the fiber, consecutively. The purity of few OAM modes is evaluated in the 0.9 μm wavelength band (since 0.9 μm wavelength occurs the lowest confinement loss) and the outcomes are portrayed in Fig. 4. The findings show that the purity of the EH mode is lower than that of the HE mode for the same OAM mode sequence. In the proposed fiber, the purity of OAM modes is approximately $>96\%$ and the highest purity reaches up to 99.31792% for the $HE_{6,1}$ mode. Therefore, the large amounts of OAM modes with remarkable OAM purity-based anti-resonant fiber provide a significant effect on the application of MDM technology.

3.3. Effective refractive index (ERI)

The ERI of various OAM modes of the designed anti-resonant fiber with respect to wavelength is demonstrated in Fig. 5. This fiber, only a single type of SF2 material is used within the circular tubes and annular region (which confined the OAM modes). Therefore, the ERI of the SF2 material is calculated using the Sellmeier equation [28] and expressed as Eq. (4) [29]:

$$n(\lambda) = \sqrt{1 + \sum_{i=1}^{3} \frac{A_i \lambda^2}{\lambda^2 - B_i}} \tag{4}$$

here 'λ' define the operating wavelength of the presented fiber, A_i and B_i denote the Sellmeier coefficients of the doped material (SF2) [29]. In Fig. 5, the results show that the ERI is thinly downfall with enhancing the wavelength over the 400 nm bandwidth. Additionally, it is noted that higher-order OAM modes have a lower ERI, and the EH mode has a greater RI than the HE mode at identical OAM orders. The ERI also has an effect on the planned fiber's waveguide dispersion properties.

3.4. Effective refractive index differences (ERIDs)

To contain the OAM modes in the designed anti-resonant fiber, a precondition is that ERIDs within the HE and EH modes must be above10^{-4}, else LP mode will have occurred that provide the large crosstalk among the channel. So, the detachment between the vector modes can be expressed as the following equation [26]:

$$\Delta n_{eff} = \left| n_{eff_{HE_{l+1,m}}} - n_{eff_{EH_{l-1,m}}} \right| > 10^{-4} \tag{5}$$

where 'Δn_{eff}' defines the ERIDs between the vector modes. The simulated ERIDs of the several OAM mode is displayed in Fig. 6 within the 0.6 μm to 1.0 μm wavelength. Furthermore, the ERIDs of the raised model are gently increasing for the higher-order OAM modes. In this Figure, a green straight line is used for 10^{-4} and the results show that all the ERIDs are above the mentioned line. For this reason, the LP mode generation has been suppressed and the crosstalk of optical fiber communication systems is decreases by the proposed anti-resonant fiber.

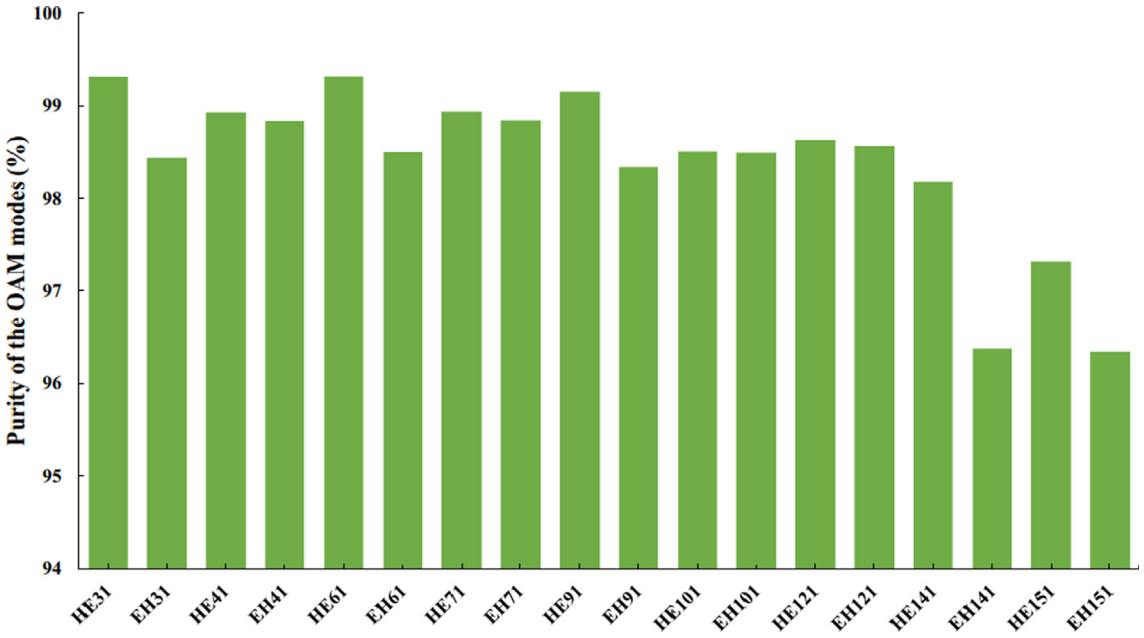

Fig. 4 Several OAM mode purity of the anti-resonant fiber.

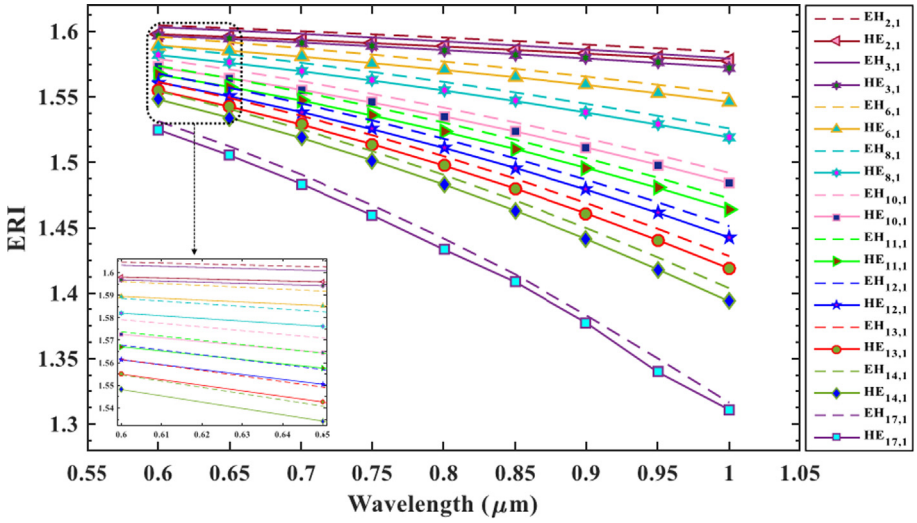

Fig. 5 ERI with wavelength of the anti-resonant fiber. The inset depicts the explicit scene of the dash-shaped location highlighted.

3.5. Chromatic dispersion

The dispersion is an essential characteristic of the anti-resonant OAM fiber in the transmission of information because flat and low dispersion assures fast propagation in the fiber. Additionally, flat and ultra-low dispersion-based OAM fiber can be used to simultaneously transmit numerous signals and to actualize long-distance broadband signal transmission. The suggested fiber's dispersion profile can be described using the following formula, Eq. (6) [26]:

$$D = D_m + D_w = -\frac{\lambda}{c}\frac{d^2 n[\lambda]}{d\lambda^2} - \frac{\lambda}{c}\frac{d^2 Re[n_{eff}]}{d\lambda^2} \tag{6}$$

where 'D_m', 'D_w', and 'c' indicate the material dispersion, the waveguide dispersion, and the velocity of light in a vacuum, consecutively. Material dispersion is a small effect on the chromatic dispersion and due to this, only waveguide dispersion is considered of the designed anti-resonant fiber. Besides, Fig. 7 demonstrates the relationship between the dispersion and the operating wavelength of the designed fiber. The lower-order OAM modes provide the low and flattened dispersion trend while the higher-order OAM mode varies greatly from the proposed anti-resonant fiber which is clearly understood through Fig. 7. It is also observed that in the corresponding order of OAM modes, the HE mode has relatively larger dispersion than the EH mode. The simulated dispersion variation of some OAM modes is shown in Table 2. Therefore, ultra-low and flattened dispersion-based lower-order OAM modes enhance the quick propagation of information within the fiber.

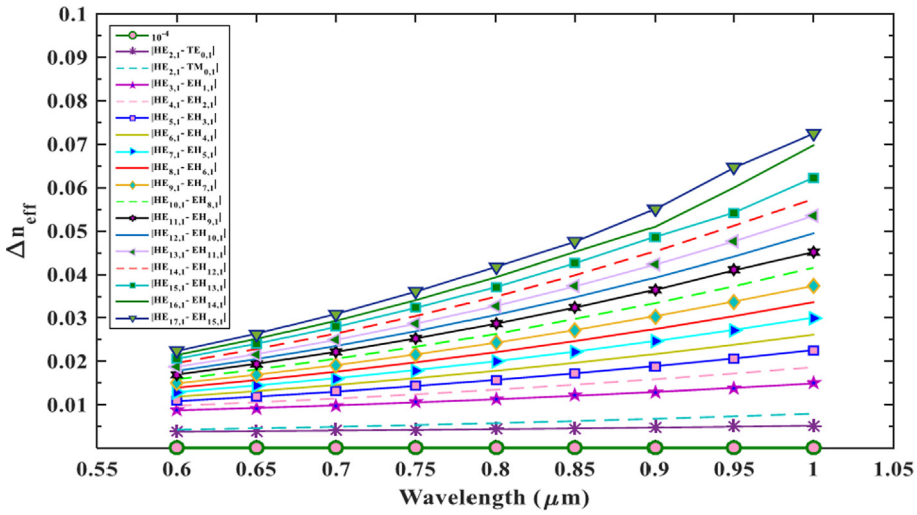

Fig. 6 ERIDs with wavelength of the anti-resonant fiber.

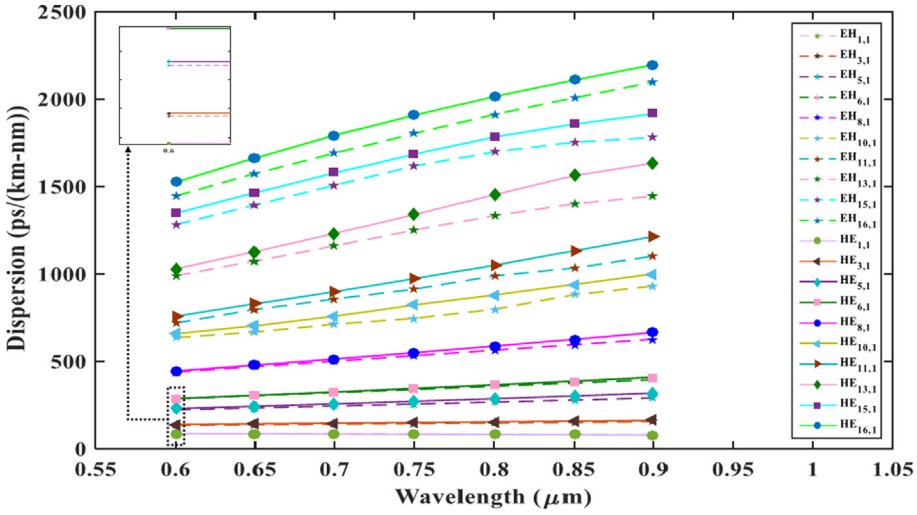

Fig. 7 Dispersion with wavelength of the anti-resonant fiber. The inset depicts the explicit scene of the dash-shaped location highlighted.

Table 2 Several dispersion variations of OAM modes are supported by the proposed fiber.

OAM modes	$HE_{1,1}$	$HE_{3,1}$	$HE_{5,1}$	$HE_{6,1}$	$HE_{11,1}$	$HE_{13,1}$	$HE_{15,1}$	$HE_{16,1}$
Dispersion variation (ps/km-nm)	−8.765	23.122	88.657	122.172	455.7	605.1	568.7	671.7
OAM modes	$EH_{1,1}$	$EH_{3,1}$	$EH_{5,1}$	$EH_{6,1}$	$EH_{11,1}$	$EH_{13,1}$	$EH_{15,1}$	$EH_{16,1}$
Dispersion variation (ps/km-nm)	−8.838	21.358	68.203	107.768	383.1	455.8	499	652.7

3.6. Effective mode field area (EMA)

EMA (A_{eff}) gives a significant impact on the transmission of OAM modes. It also provides an effective influence on the numerical aperture properties. The mode field area can be measured through the following expression (7) [30]:

$$A_{eff} = \frac{\left(\iint |E(x,y)|^2 dxdy\right)^2}{\iint |E(x,y)|^4 dxdy} \tag{7}$$

where '$E(x,y)$' define the mode power of the electric field distribution. The annular region and the ERIDs of the fiber [31] affect the size of the mode field area. The calculated results of the A_{eff} with respect to the wavelength of the designed anti-resonant fiber are displayed in Fig. 8. Moreover, the result shows that higher-order OAM modes provide a lower effective field area because the light intensity is easily leaked to the cladding region of the higher-order modes. Also, the effective area is slowly increased by raising the controlling wavelength and the durability of the higher-order OAM modes used to transmit in optical communications.

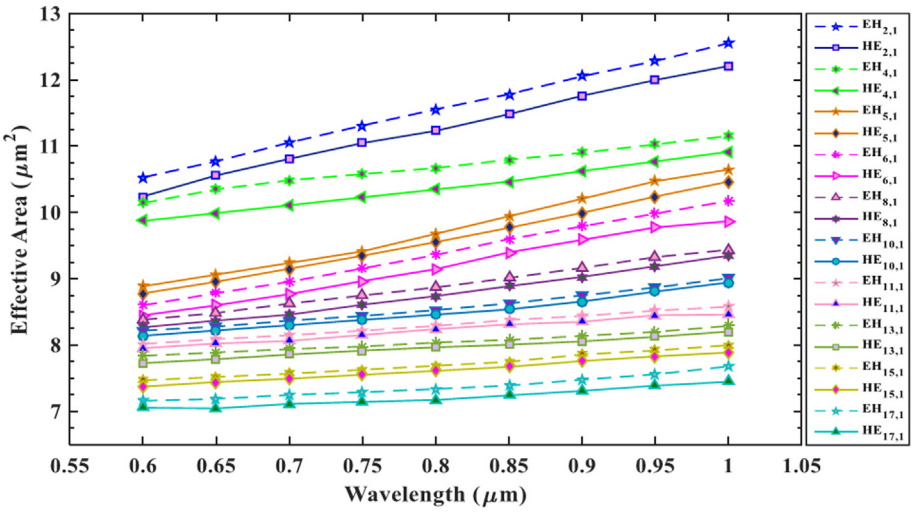

Fig. 8 Effective field area with wavelength of the anti-resonant fiber.

3.7. Numerical aperture (NA)

The total assumption of light rays or power in the anti-resonant fiber is measured by the NA characteristic. It is a unit-less parameter and can be expressed through Eq. (8) [26]:

$$\mathrm{NA} = \left[1 + \frac{\pi A_{eff}}{\lambda^2}\right]^{-\frac{1}{2}} \tag{8}$$

The relationship between the NA and the wavelength is positively correlated with the proposed model which is depicted in Fig. 9. This figure shows that the NA is politely increased with raising the order of OAM modes between the 0.6 μm and 1.0 μm wavelength and the maximum NA have been obtained where the minimum effective area occurs. The highest value has been obtained by the proposed anti-resonant fiber is 0.20245 (for the $HE_{17,1}$ mode) and the fiber is mostly used in the field of medical imaging as well as optical coherence tomography (OCT).

3.8. Confinement loss (CL)

When OAM mode is transmitted through the anti-resonant fiber, some of the OAM modes are leakage through the cladding area due to the several structural designs, which phenomenon will occur in the CL. It is one of the destructive parameters that immediately collapse the distance of transmission. Therefore, lower CL is favorable to the transmission of OAM modes into the fiber with low loss. The CL of the fiber is mathematically calculated as the following expression [29]:

$$C_{loss} = \frac{2\pi}{\lambda}\frac{20}{\ln(10)}10^6 Im(n_{eff})(dB/m) \tag{9}$$

where 'λ' and '$Im(n_{eff})$' represent the controlling wavelength and the imaginary part of the proposed structure, respectively. Fig. 10 shows that the wavelength of the proposed fiber could be over the 400 nm bandwidth within the CL of some OAM mode. The CL of the supported modes shows the explicit

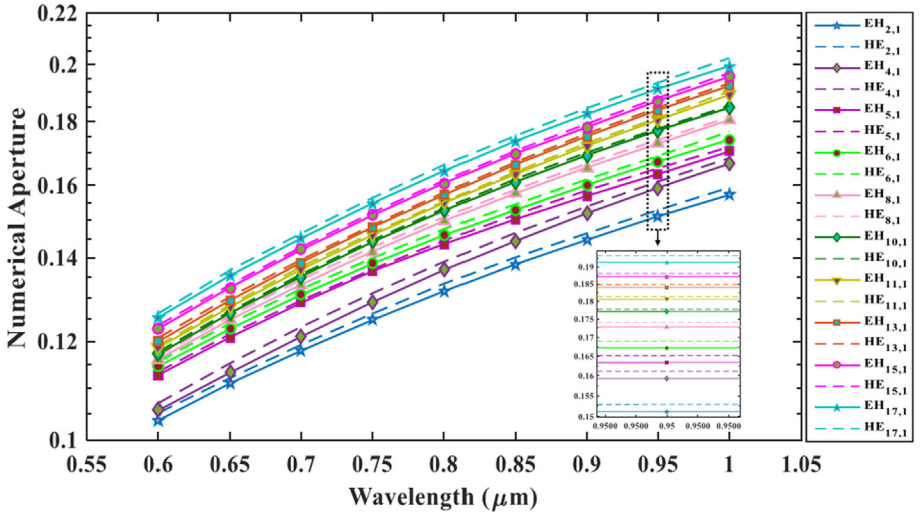

Fig. 9 NA with wavelength of the anti-resonant fiber. The inset depicts the explicit scene of the dash-shaped location highlighted.

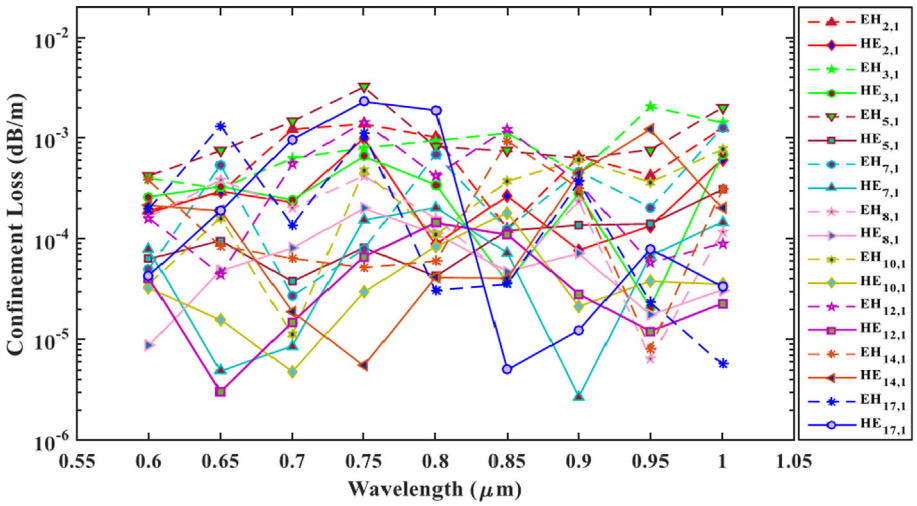

Fig. 10 CL with wavelength of the anti-resonant fiber.

Table 3 Comparative analysis of the designed anti-resonant fiber with other published OAM fibers.

Ref.	OAM Mode Number	Confinement Loss (dB/m)	Material Applied	Structure Type
[1]	28	10^{-13}	Silica	NCF
[23]	56	$< 10^{-8}$	SF6	PCF
[27]	42	9.52×10^{-9}	Silica	PCF
[33]	22	10^{-10}	Silica	NCF
[34]	38	$10^{-10} - 10^{-9}$	As_2S_3	Hollow-core ring PCF
This Fiber	**64**	$\mathbf{2.7031 \times 10^{-6}}$	**SF2**	**Anti-resonant Fiber**

zigzag trends. When the cladding mode's ERI is close to the value of the objective mode, the cladding mode's phase exhibits a zigzag intensity distribution [32]. In Fig. 10, the CL of the permitted OAM modes is approximately varied between the 5.7031×10^{-5} dB/m to 9.2537×10^{-4} dB/m. Also, the minimum CL of the designed structure is 2.7031×10^{-6} dB/m for the $HE_{7,1}$ mode at the 900 nm wavelength. Therefore, the main convenience of the low confinement loss provides stable OAM transmission and a potential candidate in fiber communications.

Based on the above discussion, Table 3 exhibits the performance evaluation of the presented anti-resonant fiber with the other related OAM fiber. The designed single material-based anti-resonant fiber provides a large number of OAM modes, better OAM purity, low CL, and flat dispersion variations which shows the potential applications in OAM transmission, high quality, and long-distance fiber communication.

4. Conclusion

The proposed anti-resonant fiber structure can be fabricated by the modified chemical vapor deposition (MCVD) and fiber drawing facilities. To generate the appropriate preform geometry, sufficient concentrations of SiO_2 and GeO_2 are accumulated to produce the ring core annular region in front of resembling the index profile cladding [35–37]. Then, the circular tubes of the cladding region (inner and outer layers) are collapsed to create the glass preform. Finally, the fiber drawing scheme controls the annular region diameter in order to produce the fiber's predicted geometry. As a result, the proposed anti-resonant fiber will be constructed first, followed by studies to evaluate the structure's propagation characteristics.

Overall, It could be concluded saying that the outcomes of the proposed fiber depict that the ERIDs of the vector modes are $> 10^{-4}$ which suppress the generation of LP mode and only provide the OAM mode in the annular region. Other optical properties including low and flat dispersion (-8.838 ps/km-nm) assure the fast propagation among the fiber, high OAM purity (99%) ascertains the efficient transmission of information, and used in the MDM technology, lower confinement loss (2.7031×10^{-6} dB/m) is fortunate to the OAM modes transmission within the fiber with low loss. Finally, we expected that the proposed anti-resonant fiber might be a potential impact on the transmission of the OAM on large-capacity-based long-distance communications.

Thus, in the summarization, we have designed a novel anti-resonant fiber that supports a large amount of OAM mode that is why it is suitable for long-distance communications. All the propagation characteristics of the fiber have been numerically calculated through the FEM and PML in the COMSOL Multiphysics simulator. We want to emphasis here that we do theoretical/computational studies. However, there are limitations of this study, for example, data collection process and experimental facility. So, one may extend this study to study about the different types of air-hole tube arrangement in

the cladding part as well as doping the core materials with a deep investigation and we are more than happy to collaborate, if invited.

Funding

This work was supported by the Deanship of Scientific Research at Umm Al-Qura University by Grant Code: (22UQU4170008DSR01). This work was also supported in part by funding from the Natural Sciences and Engineering Research Council of Canada (NSERC).

Declaration of Competing Interest

The authors declare that they have no known competing financial interests or personal relationships that could have appeared to influence the work reported in this paper.

Acknowledgements

This work was supported by the Deanship of Scientific Research at Umm Al-Qura University for supporting this work by Grant Code: (22UQU4170008DSR02).

References

[1] J. Tu, Z. Liu, S. Gao, Z. Wang, J. Zhang, B. Zhang, J. Li, W. Liu, H. Tam, Z. Li, C. Yu, C. Lu, Ring-core fiber with negative curvature structure supporting orbital angular momentum modes, Opt. Express 27 (15) (2019) 20358, https://doi.org/10.1364/OE.27.020358.

[2] S. Hong, Y.S. Lee, H. Choi, C. Quan, Y. Li, S. Kim, K. Oh, Hollow silica photonic crystal fiber guiding 101 orbital angular momentum modes without phase distortion in C+ L band, J. Lightwave Technol. 38 (5) (2020) 1010–1018.

[3] R.G.H. van Uden, R.A. Correa, E.A. Lopez, F.M. Huijskens, C. Xia, G. Li, A. Schülzgen, H. de Waardt, A.M.J. Koonen, C. M. Okonkwo, Ultra-high-density spatial division multiplexing with a few-mode multicore fibre, Nat. Photonics 8 (11) (2014) 865–870.

[4] F.A. Al-Zahrani, Estimating the Survivability Impact of Multi-Fiber Wavelength-Division Multiplexing Networks, IEEE Access 8 (2020) 202387–202400.

[5] M.E. Friese, T.A. Nieminen, N.R. Heckenberg, H. Rubinsztein-Dunlop, Optical alignment and spinning of laser-trapped microscopic particles, Nature 394 (6691) (1998) 348–350.

[6] K. Dholakia, T. Čižmár, Shaping the future of manipulation, Nat. Photonics 5 (6) (2011) 335–342.

[7] G.A. Swartzlander, E.L. Ford, R.S. Abdul-Malik, L.M. Close, M.A. Peters, D.M. Palacios, D.W. Wilson, Astronomical demonstration of an optical vortex coronagraph, Opt. Express 16 (14) (2008) 10200–10207.

[8] G. Xie, H. Song, Z. Zhao, G. Milione, Y. Ren, C. Liu, R. Zhang, C. Bao, L. Li, Z. Wang, K. Pang, D. Starodubov, B. Lynn, M. Tur, A.E. Willner, Using a complex optical orbital-angular-momentum spectrum to measure object parameters, Opt. Lett. 42 (21) (2017) 4482, https://doi.org/10.1364/OL.42.004482.

[9] A.E. Willner, H. Huang, Y. Yan, Y. Ren, N. Ahmed, G. Xie, C. Bao, L. Li, Y. Cao, Z. Zhao, J. Wang, M.P.J. Lavery, M. Tur, S. Ramachandran, A.F. Molisch, N. Ashrafi, S. Ashrafi, Optical communications using orbital angular momentum beams, Adv. Opt. Photonics 7 (1) (2015) 66, https://doi.org/10.1364/AOP.7.000066.

[10] A. Trichili, K.-H. Park, M. Zghal, B.S. Ooi, M.-S. Alouini, Communicating using spatial mode multiplexing: potentials, challenges, and perspectives, IEEE Commun. Surv. Tutorials 21 (4) (2019) 3175–3203.

[11] G. Zhu, Z. Hu, X. Wu, C. Du, W. Luo, Y. Chen, X. Cai, J. Liu, J. Zhu, S. Yu, Scalable mode division multiplexed transmission over a 10-km ring-core fiber using high-order orbital angular momentum modes, Opt. Express 26 (2) (2018) 594–604.

[12] K. Ingerslev, P. Gregg, M. Galili, F. Da Ros, H. Hu, F. Bao, M. A. Usuga Castaneda, P. Kristensen, A. Rubano, L. Marrucci, K. Rottwitt, T. Morioka, S. Ramachandran, L.K. Oxenløwe, 12 mode, WDM, MIMO-free orbital angular momentum transmission, Opt. Express 26 (16) (2018) 20225, https://doi.org/10.1364/OE.26.020225.

[13] H. Yu, P. Li, L. Zhang, Y. Zhu, F. Ahmad Al-Zahrani, K. Ahmed, Application of optical fiber nanotechnology in power communication transmission, Alexandria Eng. J. 59 (6) (2020) 5019–5030.

[14] Y. Yue, Y. Yan, N. Ahmed, J.Y. Yang, L. Zhang, Y. Ren, H. Huang, K.M. Birnbaum, B.I. Erkmen, S. Dolinar, M. Tur, Mode properties and propagation effects of optical orbital angular momentum (OAM) modes in a ring fiber, IEEE Photonics J. 4 (2) (2012) 535–543.

[15] G. Rajchakit, P. Agarwal, S. Ramalingam, Stability Analysis of Neural Networks, 2021.

[16] Y. Zhang, P. Agarwal, V. Bhatnagar, S. Balochian, J. Yan, Swarm intelligence and its applications, Sci. World J. 2013 (2013) 1–3.

[17] Y. Zhang, P. Agarwal, V. Bhatnagar, S. Balochian, X. Zhang, Swarm Intelligence and Its Applications 2014, Scientific World J. 2014 (2014) 1–4.

[18] C. Brunet, P. Vaity, Y. Messaddeq, S. LaRochelle, L.A. Rusch, Design, fabrication and validation of an OAM fiber supporting 36 states, Opt. Express 22 (21) (2014) 26117–26127.

[19] T. Fujisawa, K. Saitoh, Geometric-phase-induced arbitrary polarization and orbital angular momentum generation in helically twisted birefringent photonic crystal fiber, Photonics Res. 8 (8) (2020) 1278–1288.

[20] W. Geng, Y. Li, Y. Fang, Y. Wang, C. Bao, Y. Yan, Z. Wang, W. Zhang, H. Huang, Y. Ren, Z. Pan, Y. Yue, Highly dispersive coupled ring-core fiber for orbital angular momentum modes, Appl. Phys. Lett. 117 (19) (2020) 191101, https://doi.org/10.1063/5.0025615.

[21] T. He, B. Wu, Low confinement loss photonic crystal fibre capable of supporting 54 orbital angular momentum modes, J. Mod. Opt. 67 (6) (2020) 556–562.

[22] M.F. Israk, M.A. Razzak, K. Ahmed, M.M. Hassan, M.A. Kabir, M.N. Hossain, B.K. Paul, V. Dhasarathan, Ring-based coil structure photonic crystal fiber for transmission of Orbital Angular Momentum with large bandwidth: outline, investigation and analysis, Opt. Commun. 473 (2020) 126003, https://doi.org/10.1016/j.optcom.2020.126003.

[23] W. Wang, N. Wang, K. Li, Z. Geng, H. Jia, A novel dual guided modes regions photonic crystal fiber with low crosstalk supporting 56 OAM modes and 4 LP modes, Opt. Fiber Technol. 57 (2020) 102213, https://doi.org/10.1016/j.yofte.2020.102213.

[24] H. Wang, Y. Liang, X. Zhang, S. Chen, L. Shen, L. Zhang, J. Luo, J. Wang, Low-loss Orbital Angular Momentum ring-core fiber: design, fabrication and characterization, J. Lightwave Technol. 38 (22) (2020) 6327–6333.

[25] S.F. Gao, Y.Y. Wang, W. Ding, D.L. Jiang, S. Gu, X. Zhang, P. Wang, Hollow-core conjoined-tube negative-curvature fibre with ultralow loss, Nat. Commun. 9 (1) (2018) 1–6.

[26] M.M. Hassan, M.A. Kabir, M.N. Hossain, B. Biswas, B.K. Paul, K. Ahmed, Photonic crystal fiber for robust orbital angular momentum transmission: design and investigation, Opt. Quant. Electron. 52 (1) (2020) 8.

[27] H. Zhang, X. Zhang, H. Li, Y. Deng, X. Zhang, L. Xi, X. Tang, W. Zhang, A design strategy of the circular photonic crystal fiber supporting good quality orbital angular momentum mode transmission, Opt. Commun. 397 (2017) 59–66.
[28] M.A. Kabir, M.M. Hassan, M.N. Hossain, B.K. Paul, K. Ahmed, Design and performance evaluation of photonic crystal fibers of supporting orbital angular momentum states in optical transmission, Opt. Commun. 467 (2020) 125731, https://doi.org/10.1016/j.optcom.2020.125731.
[29] F.A. Al-Zahrani, K. Ahmed, Novel design of dual guided photonic crystal fiber for large capacity transmission in high-speed optics communications with supporting good quality OAM and LP modes, Alexandria Eng. J. 59 (6) (2020) 4889–4899.
[30] W. Tian, H. Zhang, X. Zhang, L. Xi, W. Zhang, X. Tang, A circular photonic crystal fiber supporting 26 OAM modes, Opt. Fiber Technol. 30 (2016) 184–189.
[31] M. Xu, G. Zhou, C. Chen, G. Zhou, Z. Sheng, Z. Hou, C. Xia, A novel micro-structured fiber for OAM mode and LP mode simultaneous transmission, J. Opt. 47 (4) (2018) 428–436.
[32] C. Wei, R.J. Weiblen, C.R. Menyuk, J. Hu, Negative curvature fibers, Adv. Opt. Photonics 9 (3) (2017) 504–561.
[33] J. Tu, S. Gao, Z. Wang, Z. Liu, W. Li, C. Du, W. Liu, Z. Li, C. Yu, H. Tam, C. Lu, Bend-insensitive grapefruit-type holey ring-core fiber for weakly-coupled OAM mode division multiplexing transmission, J. Lightwave Technol. 38 (16) (2020) 4497–4503.
[34] C. Jia, H. Jia, N. Wang, J. Chai, X. Xu, Y. Lei, G. Liu, Y. Peng, J. Xie, Theoretical analysis of a 750-nm bandwidth hollow-core ring photonic crystal fiber with a graded structure for transporting 38 orbital angular momentum modes, IEEE Access 6 (2018) 20291–20297.
[35] S. Pilz, H. Najafi, M. Ryser, V. Romano, Granulated silica method for the fiber preform production, Fibers 5 (24) (2017) 1–19.
[36] R. Camassa, M.G. Forest, L. Lee, H.R. Ogrosky, J. Olander, Ring waves as a mass transport mechanism in air-driven core-annular flows, Phys. Rev. E 86 (2012) 066305.
[37] R. Osellame, G. Cerullo, R. Ramponi, Femtosecond Laser Micromachining, Springer, Berlin, Heidelberg, 2012.